Supplementary Information

Hard confinement systems as effective *'nanoreactors'* for *'in-situ'* photo-RAFT: Towards control over molecular weight distribution and morphology

Roksana Bernat[1,2], Paulina Maksym[2,3]*, Magdalena Tarnacka[2,3], Anna Szelwicka[4], Rafał Bielas[2,3], Marcin Wojtyniak[2,3], Katarzyna Balin[2,3], Barbara Hachuła[1,2], Anna Chrobok[4], Marian Paluch,[2,3] Kamil Kamiński[2,3]

[1] *Institute of Chemistry, University of Silesia, ul. Szkolna 9, 40-007 Katowice, Poland*

[2] *Silesian Center of Education and Interdisciplinary Research, University of Silesia, ul. 75 Pulku Piechoty 1A, 41-500 Chorzow, Poland*

[3] *Institute of Physics, University of Silesia, 75 Pułku Piechoty 1, 41-500 Chorzów, Poland*

[4] *Department of Chemical Organic Technology and Petrochemistry, Silesian University of Technology, Krzywoustego 4, 44-100 Gliwice, Poland*

*****Corresponding author: e-mail* paulina.maksym@smcebi.edu.pl

1. Materials

Methyl methacrylate (MMA, >99%, Sigma Aldrich), Cyanomethyl methyl(4-pyridyl)carbamodithioate (CTA1, 98%, Sigma Aldrich), 2-(Dodecylthiocarbonothioylthio)-2-methylpropionic acid (CTA2, 98%, Sigma Aldrich), Tris[2-(dimethylamino)ethyl]amine (Me_6TREN, 97%, Sigma Aldrich), 1-vinyl-1,2,4-triazole (>97%, Sigma Aldrich), methyl iodide (>99%, Acros), lithium bis(trifluoromethanesulfonimide) (>99%, Acros), 2,4-dimethylphenol (>99, Acros), dimethyl sulfoxide (DMSO, 98%, Chempur), methanol (98%, Chempur), chloroform (98.5%, Chempur), chloroform-d (Sigma Aldrich), Mesoporous silica molecular sieve SBA-15 (SBA-15, ACS Material) were used as received. In the experiment, we also used membranes with different pore diameters: silica – 4 nm (self-made systems) and alumina 10 nm (commercialy-available Synkera).

Photo-RAFT experiments were carried out in hard confinement systems differing in form, composition, pore arrangement, diameters, thickness and transparency. For that purpose, we selected commercial MOF powder SBA-15 (SiO_2; irregular pore arrangement, pore diameter d=5-15 nm) *ii)* commercial AAO-based templates (regular pore arrangement, pore diameter d=10 nm) and *iii)* self-produced SiO_2-based templates (regular pore arrangement, pore diameter d=4 nm).

MOF (SBA-15) possesses frameworks of uniform hexagonal pores of tunable diameter (5 nm do 15 nm), narrow distribution of their sizes and relatively thick walls (ranges between 3.1 and 6.4 nm).

Native silica membranes were prepared as presented in Ref. [1] by electrochemical etching of highly doped p-type <100> oriented silicon wafers with resistivity ≤ 0.005 Ω cm and thermal oxidation at 1100 K. A mixture of Hydrofluoric acid and Ethanol in the ratio of 1:1 was used as an electrolyte. Densities of j=20 $mAcm^{-1}$ were applied to obtain pore diameters of d=4 nm with the porosity of 9-7%. Obtained membranes were 100 ± 5 μm thick. Before filling the templates, they were annealed in high vacuum (10^{-5} mbar) at 470 K for 24 h to remove any volatile impurities.

The nanoporous alumina oxide membranes used in this study (supplied from InRedox) are composed of uniaxial channels (open from both sides) with well- defined pore diameter, d ~10 ± 2 nm, thickness ~ 50 ± 2 μm and porosity ~ 12 ± 2 %. Details concerning pore density, distribution, etc. can be found at the Webpage of the producer[2].

2. Methods

2.1. N_2 adsorption/desorption isotherms.

The porosity, as well as pore diameter of SiO_2 templates (d=4nm), have been determined based on the low-temperature nitrogen adsorption/desorption isotherms measured at 77 K by using automatic ASAP 2020 sorption analyzer (Micromeritics Instrument Corp., USA). Prior to the measurement, the established amount (0.18 g) of SiO_2 (d=4 nm) support was outgassed (2 μmHg) at 453 K for 48h under vacuum in the degassing port of the sorption analyzer. The obtained adsorption/desorption isotherms were used to evaluate the structure of the studied material. Data analysis was assessed by means of MicroActive software (Micromeritics). The calculations of the pore size distribution (PSD), and the average BJH desorption pore diameter ($D_{av,des}$) and the maximum pore diameter ($D_{mo,des}$) were obtained

from the desorption branches of the nitrogen isotherm by means of the Barrett–Joyner–Halenda (BJH) procedure for cylinder pores with Halsey-Faas correction without smooth differentials[3]. The experimental nitrogen adsorption/desorption isotherms and pore-size distribution (PSD) function calculated from the desorption branch of isotherm for the investigated sample are illustrated in **Figure S1** and **Figure S2a**, respectively. The shape of isotherm (type IV according to IUPAC classification) with well-defined H1 hysteresis loops is typical for mesoporous solids with a sharp increase of adsorption at the point corresponding to the capillary condensation in mesopores.

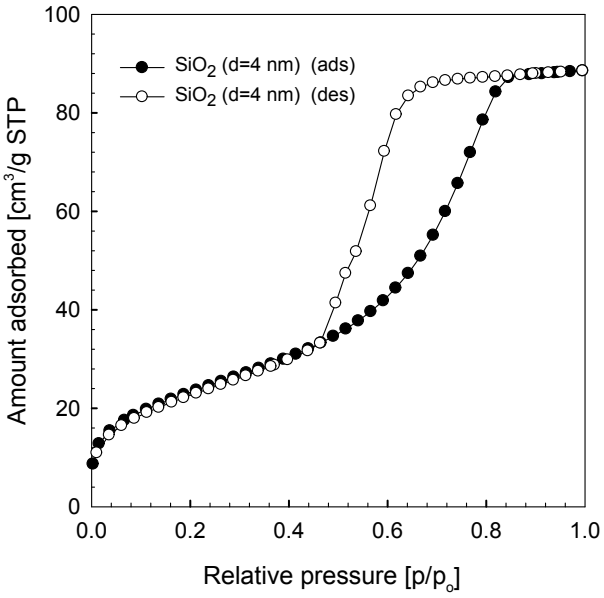

Figure S1. Nitrogen adsorption/desorption isotherms for SiO_2 material (d=4 nm).

The pore size distribution (PSD) curve for SiO_2 of d=4 nm was estimated from the desorption branch of nitrogen isotherm using the Barrett–Joyner–Halenda (BJH) model with cylindrical pores (**Figure S2a**). The PSD plot for the investigated material shows relatively narrow pore sizes distribution suggesting that porous structure is fairly uniform; the diameter of the pores is about $D_{av,des}$ ~ 4.27 nm, $D_{mo,des}$ ~ 4.50. Additionally, for characterization of SiO_2 nanopores scanning electron microscopy (SEM) measurements were performed, see **Figure S2b.**

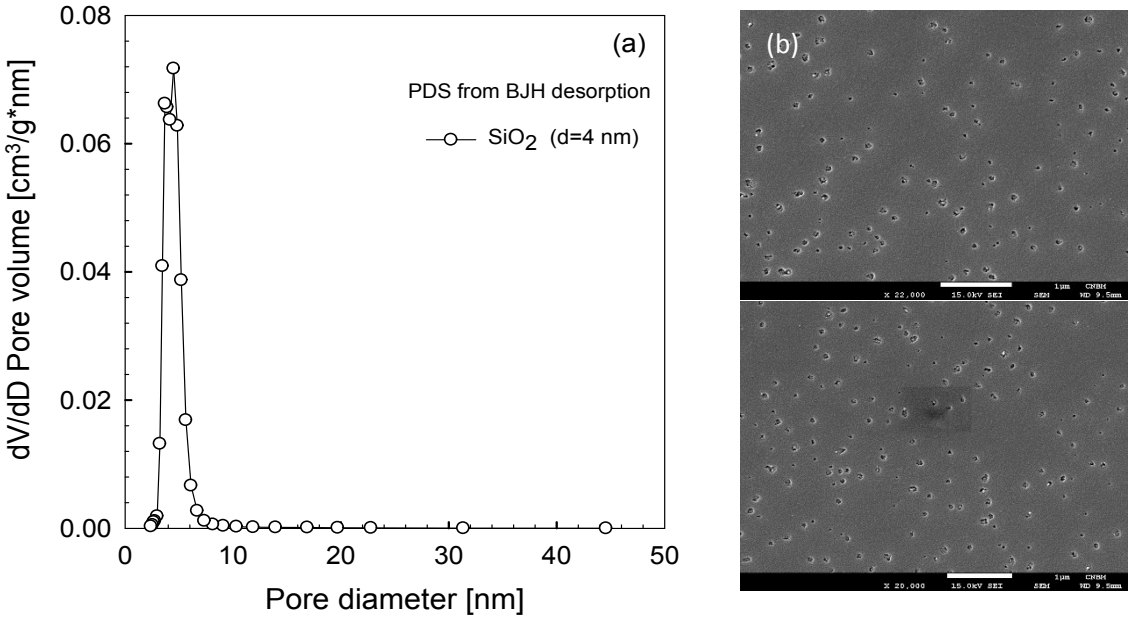

Figure S2. (a) Pore size distribution (PSD) for SiO_2 (*d*=4 nm) calculated from desorption branches of isotherm; (b) Scanning electron microscope (SEM) images for SiO_2 of *d*=4 nm.

2.2. Light absorption/emission profiles

We have used the commercially available NU-8 UV Hand Lamp from Herolab. The light source was able to produce two wavelengths of 254 and 365 nm. For our experiments, we have used 365 nm wavelength exclusively. The emission spectra for the lamp can be found in **Figure S3**. One can notice that the 365 nm wavelength possesses relatively wide distribution with FWHM parameter close to 39 nm.

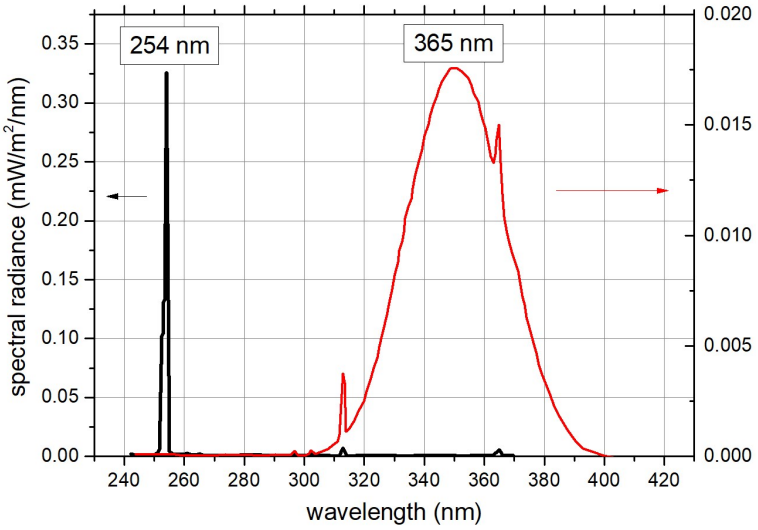

Figure S3. The emission spectra for the light source.

The implemented light source was equipped with an 8W lamp, which was able to produce 2130 μW/cm2 light intensity at a distance of 10 cm (this distance was used in our experiments). The UV-vis absorption spectra of both CTAs and tertiary amine (0.01

mmol/ml; DMSO) as well as the emission spectrum of the used light source (λ=365 nm) showing emission-absorption overlap (**Figure S4**).

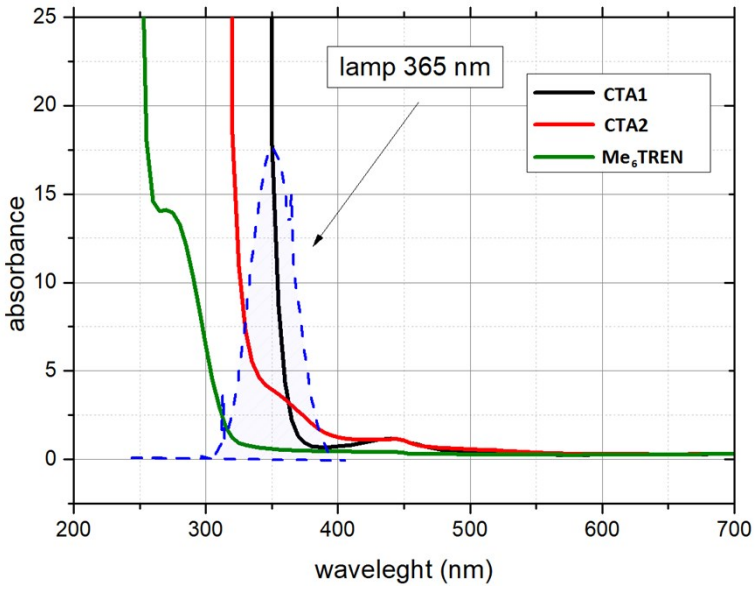

Figure S4. The UV-vis absorption spectra of both CTAs and tertiary amine (0.01 mmol/ml; DMSO) as well as the emission spectrum of the used light source.

3. Instruments

Fourier transform infrared spectroscopy (FT-IR) measurements were performed using a Nicolet iS50 FT-IR spectrometer (Thermo Scientific) equipped with an attenuated total reflectance (ATR) mode setup in the spectral range of 400 to 4000 cm^{-1}. FT-IR spectra were recorded with the spectral resolution of 4 cm^{-1} and 32 co-added scans for each spectrum.

^{1}H and ^{13}C NMR spectra were collected on Bruker Ascend 500 MHz spectrometer for the samples in $CDCl_3$ with TMS internal standard at 25 °C.

Molecular weights (M_n) and dispersities ($Đ$) of PMMA homopolymers were determined by gel permeation chromatography (GPC) with a Viscotec GPC Max VR 2001 and a Viscotec TDA 305 triple detection containing refractometer, viscosimeter and low angle laser light scattering. The OmniSec 5.12 was used for data processing. Two T6000M general mixed columns were used for separation. The measurements were carried out in THF as the solvent at 30 °C with a flow rate of 1 mL/min. The poly(ionic liquid)s and copolymer analysis were carried out in DMF with LiBr (10mmol) as the solvent at 40°C. SEC analyzes of nanomaterials were performed using special inserts.

Light source: UV hand lamp (254 and 365 nm) 8 watt tube (Herolab GmbH Laborgeräte).

Time of Flight-Secondary Ion Mass Spectrometry (TOF–SIMS) measurements were carried out with the use of TOF-SIMS.5 (ION-TOF GmbH, Munster, Germany) reflection-type spectrometer. Negative secondary ion spectra were collected by rastering the bismuth ion beam (60kV, ~0.1pA) across predetermined 500 x 500µm areas. To ensure the

maintenance of the *static* conditions, a primary ion dose was kept below 10^{12} ions/cm^2 for all samples. An electron flood gun was used to compensate charging of the sample surfaces. Both samples were measured under the same conditions with the exception of the flood gun settings. For the analysis, the SurfaceLab6.4 software was used. The negative spectra were internally mass calibrated C^-, CH^-, C_2^-, C_2H^-, C_3^- and C_3H^-.

UV-VIS measurements of the porous nanoreactors and glass batch reactor were performed using UV-VIS-NIR Microspectrophotometer from CRAIC Technologies equipped with halogen lamp and Zeiss 15x objective. The experiments were performed at room temperature and ambient pressure in the transmission geometry. The UV-VIS spectra of the other samples were obtained using UV-Vis Ratio Beam spectrophotometer from Hitachi (U-1900) equipped with standard UV quartz cuvettes.

4. Procedures

4.1. Preliminary procedures

Prior to the photo-RAFT process, both commercially-available and self-made nanoreactors were purified using the same purification procedure. First, nanoreactors were washed with different organic and inorganic solvents (water, chloroform, THF, acetone) to remove impurities formed during the templates production. Importantly, the resulting filtrates were analyzed by NMR until the impurities have been completely removed. Next, to evaporate solvents from the nanochannels, the templates were dried under vacuum at oven at 100 °C within 24 h. The commercially MOF powder (SBA-15) has been washed with acetone followed by implementation of the above-mentioned drying procedure. Note that each of polymerizations was performed with the use of brand new templates.

Each of the experiments presented in this work was repeated three times, and the results were reproducible. In addition, each process was carried out within exactly the same reaction conditions (procedure). It is worth stressing that we have used the same light source, wavelength, the distance of the light source from the reactor, volume of the incorporated reaction mixture, amount of MOF/templates, method of filling porous systems and evaporating of a non-infiltrated mixture. We also applied the same type of batch reactor for the macroscale experiments. In the case of each of nanopolymerizations brand new templates or powder (the same amount) have been utilized. Note that it was impossible to perform the chain extension experiments due to the very small amount of extracted polymer. Moreover, SEC analyzes were performed using special inserts. Herein, it should also be stressed that further routine NMR and FT-IR analysis of recovered polymers were also supported by TOF SIMS investigations

4.2. Synthesis of triazolium-based poly(ionic liquid)s

4-methyl-1-vinyl-1,2,4-triazolium bis(trifluoromethanesulfonylimide) has been synthesized according to the literature[4] *via* two-step procedure. At the first step, 1-vinyl-1,2,4-triazole (105 mmol, 10 g), methyl iodide (642 mmol, 40 ml) and 2,4-dimethylphenol (200 µl – inhibitor of the free-radical polymerisation) were introduced to the round-bottom flask. The mixture was stirred at 50 °C for 24 h and filtered off using hexane (6 x 20 ml) until

decolorization of the yellow solid - 4-methyl-1-vinyl-1,2,4-triazolium iodide (18.35 g, 77 mmol, yield=73 %).

At the second step, 4-methyl-1-vinyl-1,2,4-triazoliumbis (trifluoromethanesulfonylimide) was synthesized *via* anion exchange. 4-methyl-1-vinyl-1,2,4-triazolium iodide (18.35 g) and 2,4-dimethylphenol (200 µl) dissolved in DCM (80 ml) was introduced to the round-bottom flask. Next, lithium bis(trifluoromethanesulfonylimide) (26.5 g, 77 mmol) dissolved in deionized H_2O (60 ml) was added dropwise. The mixture was stirred at 25 °C for 24 h and transferred to the separatory funnel. Aqueous layer was washed by DCM (2 x 40 ml). Organic layers were combined and washed with deionized H_2O (8 x 40 ml) until the absence of iodide (tested using $AgNO_3$).

Description of methods:

^{1}H NMR spectra were performed at 600 MHz and ^{13}C NMR spectra were performed at 151 MHz in Varian system.

High-resolution electrospray ionisation mass spectroscopy (ESI-MS) analysis was performed applying Waters Xevo G2 QTOF apparatus equipped with an injection system (cone voltage set at 50 V; source heat up to 120 °C).

Characterization of the product:

^{1}H NMR shifts: (600 MHz, DMSO, δ, ppm): 3.72-4.06 (3H, m, -N-CH_3), 5.55 (1H, dd, H from CH_2- of the vinyl group), 6.04 (1H, dd, H from CH_2- of the vinyl group), 7.53 (1H, dd, H from -CH- of the vinyl group), 9.22 (1H, s, N^2=CH-N^4 from the triazolium ring), 10.24 (1H, s, N^1-CH=N^4 from the triazolium ring).

^{13}C NMR shifts: (151 MHz, DMSO, δ, ppm): 34.14, 109.94, 129.08, 142.25, 145.65, presence of carbon from NTf_2 anion is observed as a quartet at 112-125 ppm.

ESI-MS [M^+] spectrum of 4-methyl-1-vinyl-1,2,4-triazolium bis(trifluoromethanesulfonylimide): calc. 110.0718; found: 110.0743

ESI-MS [M^-] spectrum of 4-methyl-1-vinyl-1,2,4-triazolium bis(trifluoromethanesulfonylimide): calc. 279.9173; found: 279.9179

4.3. Photo-RAFT at the macroscale

Example of reaction with $[MetTRI/NTF]_0/[CTA1]_0$=100/1:
MetTRI (2 g, 5.1 mmol), CTA1 (0.011 g, 0.051 mmol), DMSO (2 mL) and Me_6TREN (3.4 µL, 0.012 mmol) were placed in a Schlenk flask with a magnetic stirring bar. The solution was purified by three freeze-pump-thaw cycles and purged under nitrogen. Subsequently, the mixture was transferred to the flask, placed in a chamber equipped with a magnetic stirrer and UV lamp and left to stir under light irradiation (λ=365 nm). The polymerization was stopped

after a predetermined time (5h) by turning off the light source. The polymer was isolated by precipitation into water and dried under vacuum to a constant mass.

Example of reaction with $[MMA]_0/[CTA2]_0$=100/1:
MMA (2 mL, 18.698 mmol), CTA2 (0.0661 g, 0.181 mmol) and Me_6TREN (12.5 µL, 0.047 mmol) were placed in a Schlenk flask with a magnetic stirring bar. The solution was purified by three freeze-pump-thaw cycles and purged under nitrogen. Subsequently, the mixture was transferred to the flask, placed in a chamber equipped with a magnetic stirrer and UV lamp and left to stir under light irradiation (λ=365 nm). The polymerization was stopped after a predetermined time (5h) by turning off the light source. The polymer was isolated by precipitation into cold methanol, filtered and dried under vacuum to a constant mass.

4.4. Photo-RAFT within MOF

Example of reaction with $[MMA]_0/[CTA2]_0$=100/1:
MMA (1.5 mL, 14.023 mmol), CTA2 (0.0496 g, 0.136 mmol) and Me_6TREN (9.4 µL, 0.035 mmol) were placed in a Schlenk flask. The solution was purified by three freeze-pump-thaw cycles and purged under nitrogen. Then, the reaction mixture was applied dropwise on MOF powder (0.25 g) and left to evaporate, to make sure that the polymerization was carried out within the powder nanochannels, not on its surface. The surface of filled powder was also mechanically dried using a paper towel before transferring into the Schlenk flask. Subsequently, after another purging under nitrogen, the flask was placed in a chamber equipped with a UV lamp and left under light irradiation (λ=365 nm). The polymerization was stopped after a predetermined time (5h) by turning off the light source. First, the post-reaction mixture was dissolved in $CDCl_3$ and left to wash for 1h using ultrasonic bath in order to determine the MMA consumption by ^{1}H NMR. Next, the solvent was evaporated and the polymer was isolated from the powder by precipitation into cold methanol and filtration followed by dissolving the precipitate in chloroform, re-precipitation in cold methanol and drying under vacuum to constant mass. Purified PMMA was washed with cold methanol followed by its dissolution in THF to perform SEC-LALLS measurements.

Example of reaction with $[MMA]_0/[CTA2]_0$=100/1:
MMA (1.5 mL, 14.023 mmol), CTA2 (0.0313 g, 0.140 mmol), DMSO (1.5 mL) and Me_6TREN (9.4 µL, 0.035 mmol) were placed in a Schlenk flask. The solution was purified by three freeze-pump-thaw cycles and purged under nitrogen. Then, the reaction mixture was applied dropwise on MOF (0.25 g) powder and left to evaporate, to make sure that the polymerization was carried out within the powder nanochannels, not on its surface. The surface of filled powder was also mechanically dried using a paper towel before transferring into the Schlenk flask. Subsequently, after another purging under nitrogen, the flask was placed in a chamber equipped with a UV lamp and left under light irradiation (λ=365 nm). The polymerization was stopped after a predetermined time (5h) by turning off the light source. First, the post-reaction mixture was dissolved in $CDCl_3$ and left to wash for 1h using ultrasonic bath in order to determine the MMA consumption by ^{1}H NMR. Next, the solvent was evaporated and the polymer was isolated from the powder by precipitation into cold methanol and filtration followed by dissolving the precipitate in chloroform, re-precipitation

in cold methanol and drying under vacuum to constant mass. Purified PMMA was washed with cold methanol followed by its dissolution in THF to perform SEC-LALLS measurements.

4.5. Photo-RAFT within mesoporous templates

Example of reaction with $[MMA]_0/[CTA2]_0=100/1$:

MMA (1.5 mL, 14.023 mmol), CTA2 (0.0496 g, 0.136 mmol) and Me_6TREN (9.4 µL, 0.035 mmol) were placed in a Schlenk flask. The solution was purified by three freeze-pump-thaw cycles and purged under nitrogen. The reaction mixture was transferred into a flask together with the alumina or silica templates. Then, the whole system was maintained at T=15 °C under vacuum (10^{-2} bar) for 1h to allow reagents to flow into the nanocavities. After the infiltration was completed, the surface of templates was dried mechanically with a paper towel to remove the excess of the reaction mixture, transferred to the chamber equipped with a UV lamp and left under light irradiation (λ=365 nm). The polymerization was stopped after a predetermined time by turning off the light source. First, the polymer was isolated from the template by immersing in the $CDCl_3$ and left to wash for 1h using ultrasonic bath in order to determine the MMA consumption by ^1H NMR. Next, after the template was removed, the solvent was evaporated and the polymer was precipitated into cold methanol, filtrated and dried under vacuum to constant mass. Purified PMMA was washed with cold methanol followed by its dissolution in THF to perform SEC-LALLS measurements.

5. Supplemental Figures

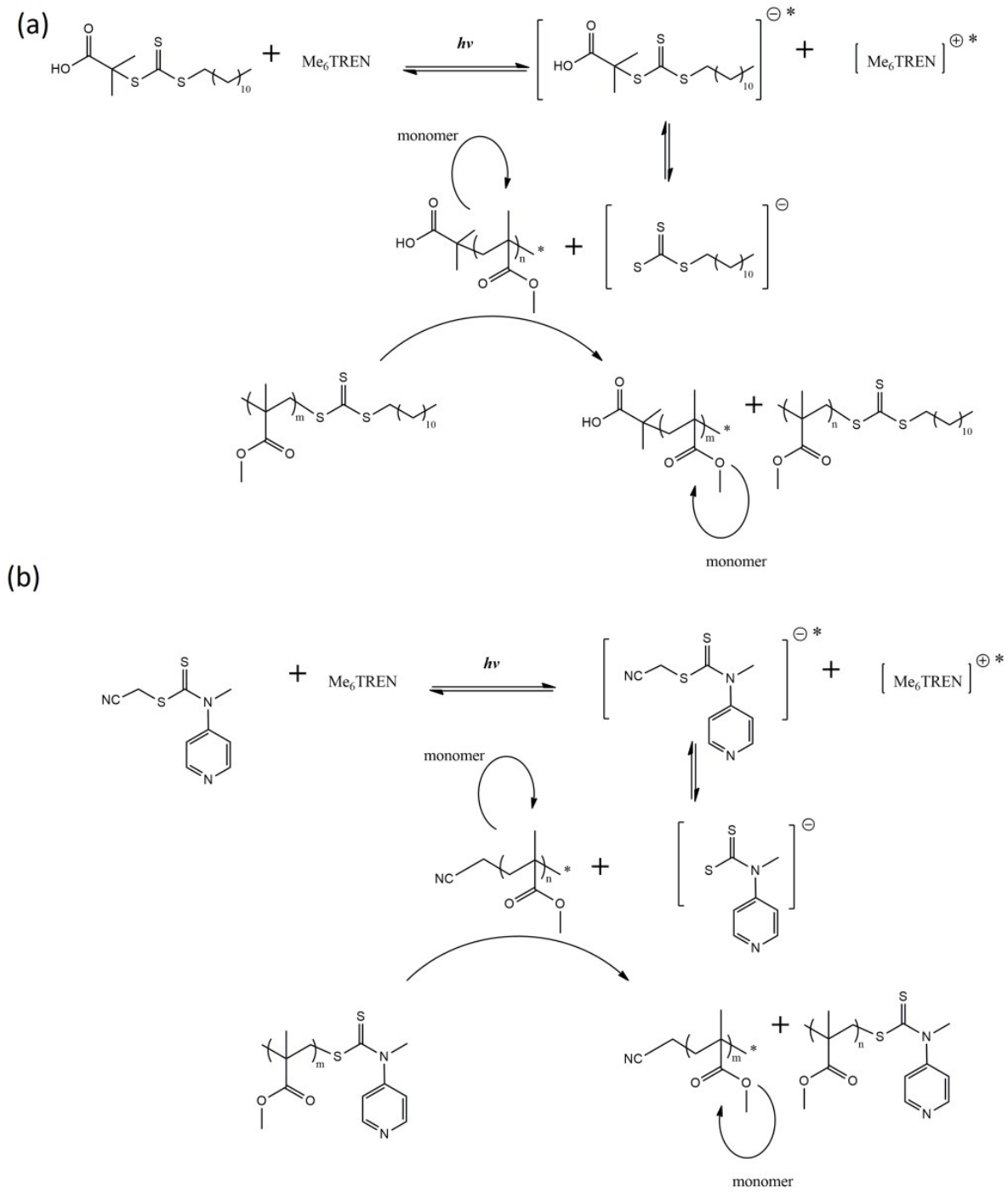

Scheme S1. Proposed mechanism of photoinferter-mediated RAFT of MMA in the presence of Me_6TREN for (a) CTA2-mediated system, and (b) CTA1-mediated system**.**

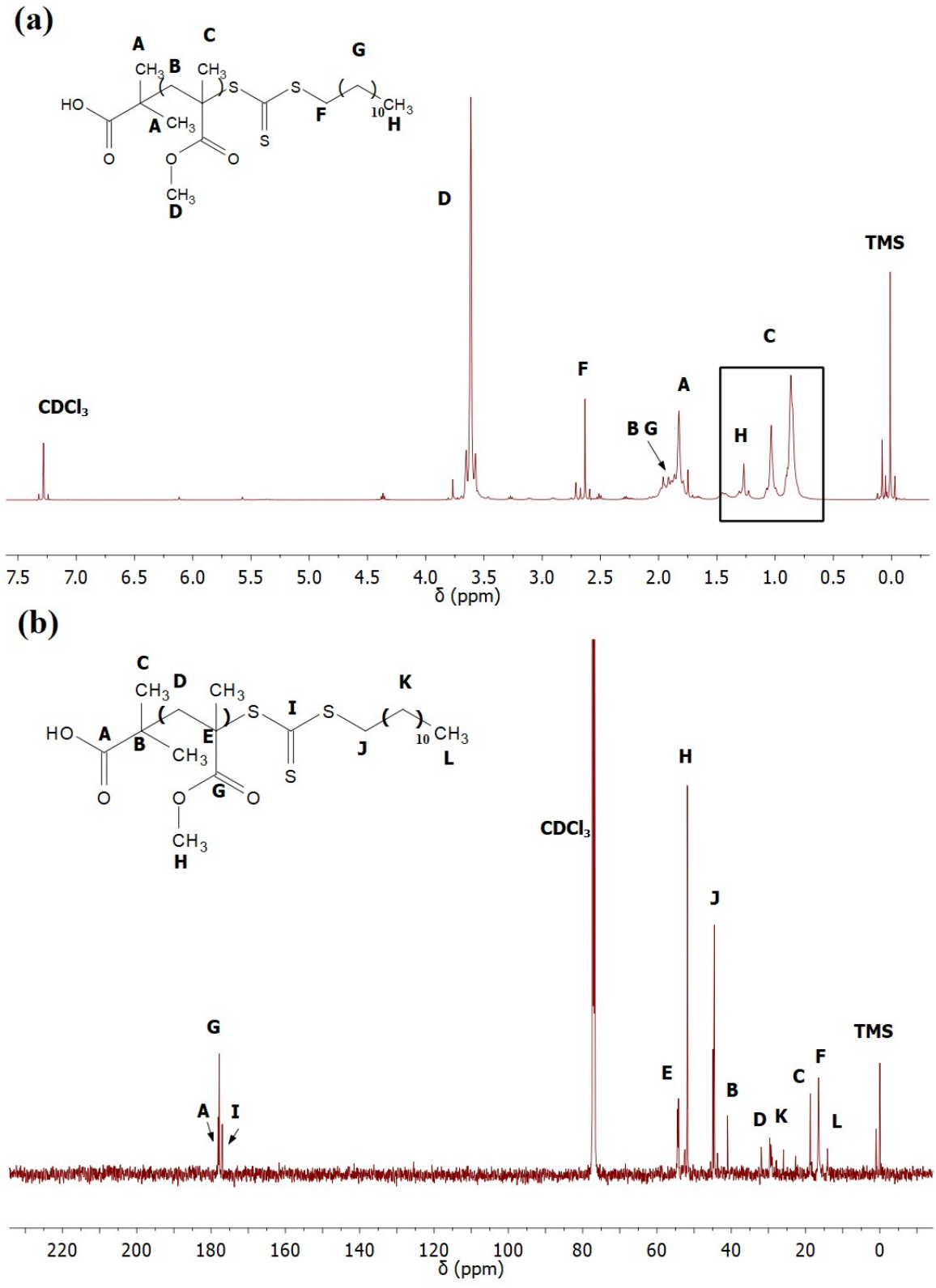

Figure S5. (A) ^{1}H and (B) ^{13}C spectrum of PMMA obtained within MOF with CTA2

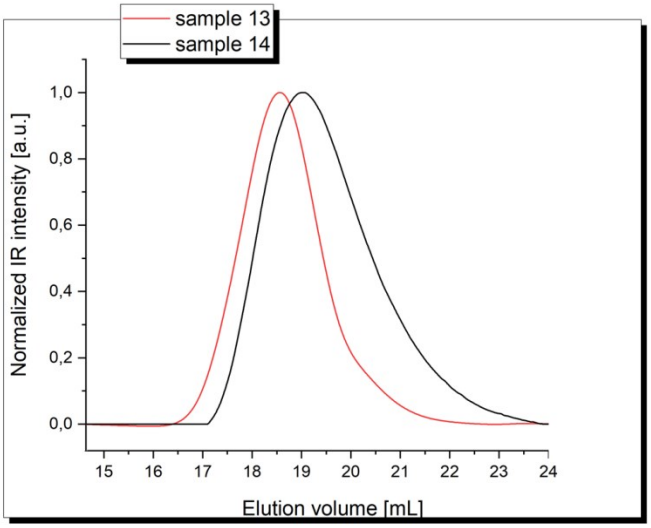

Figure S6. SEC-LALLS traces of PMMA produced under confinement via CTA2-mediated RAFT (THF)

Table S1. Chain extension experiments performed on produced macro-CTAs

no	macro-CTA	monomer	Time [h]	Conv. [%]	M_{nth} [kg/mol]	M_{nSEC}[b] [kg/mol]	Đ[b]
I*	sample 7	MMA	5	30	15.8	17.2	1.27
II	sample 2	VAc	5	22[a]	5.9	6.8	1.30
III	sample 7	VAc	5	25[a]	15.3	18.1	1.32

$[monomer]_0/[macro\text{-}CTA]_0/[Me_6TREN]_0$=50/1/0.25 (DMSO, 1/1 wt%. in respect to monomer); *addition of acid [a] determined gravimetrically, [b]SEC (DMF, LiBr as eluent)

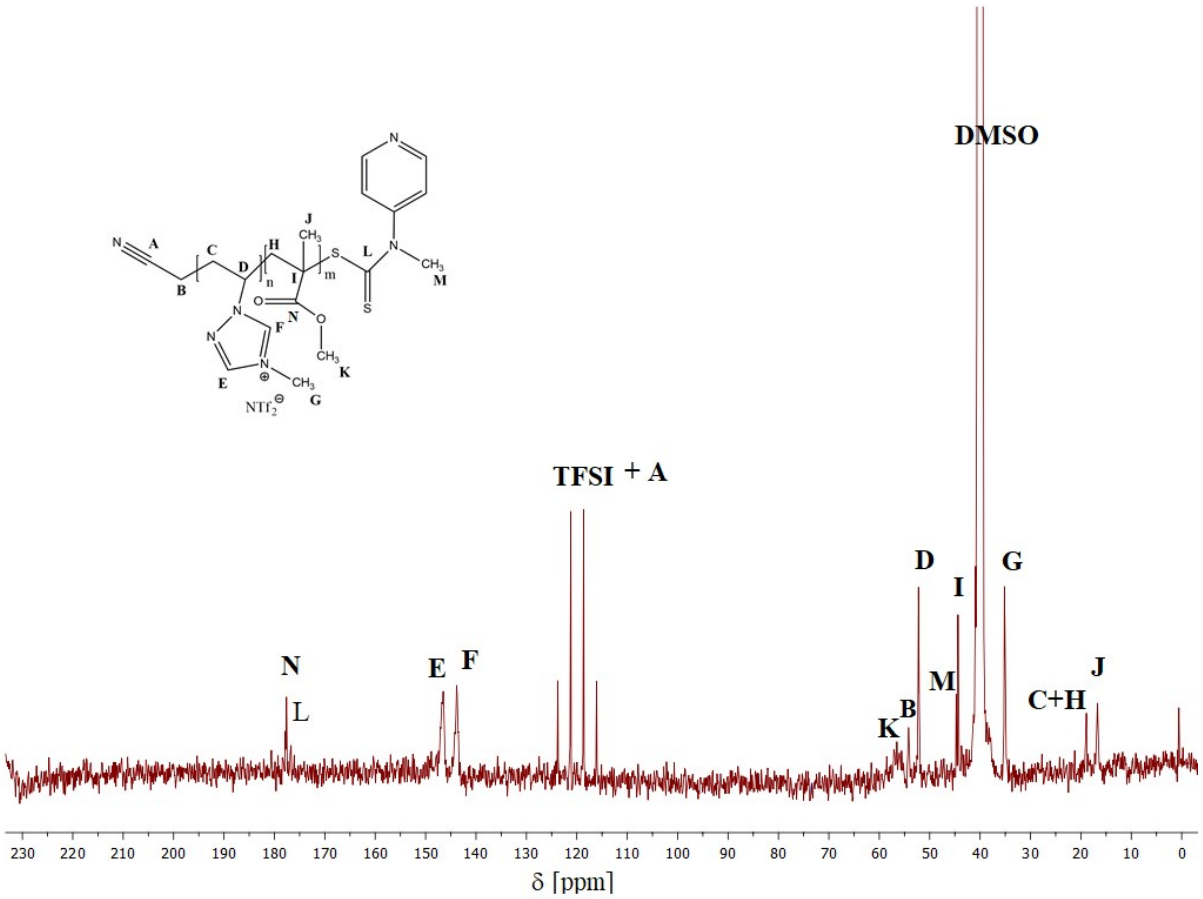

Figure S7. ^{13}C NMR spectrum of P[MetTRI/NTF]-*b*-PMMA obtained via chain extension of macro-CTA1-mediated photo RAFT (sample 7)

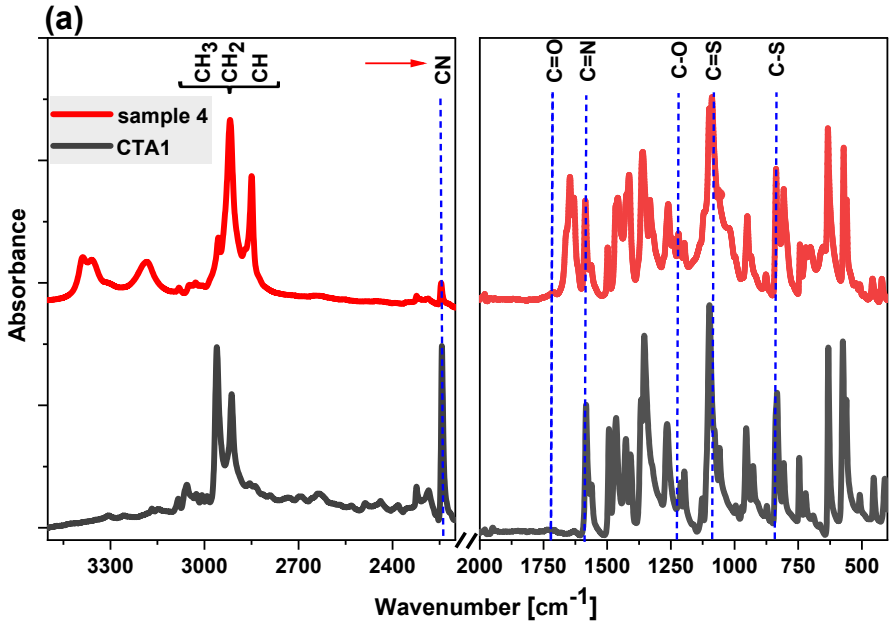

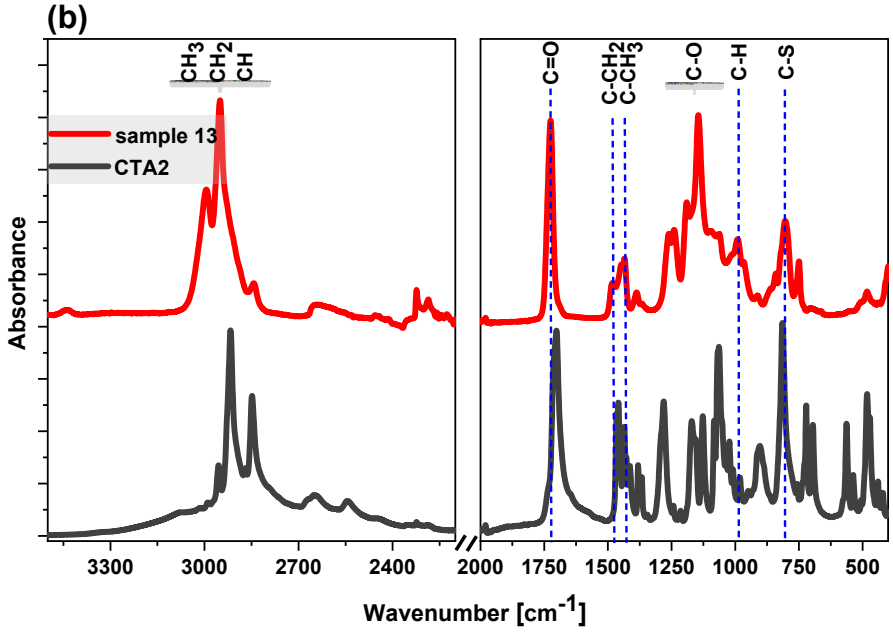

Figure S8. FTIR spectra of (a) CTA1 and PMMA produced at AAO template (*d*=10 nm) as well as (b) CTA2 and PMMA produced at AAO template (*d*=10 nm) presented in the spectral range of 3500-400 cm^{-1}.

The FT-IR spectroscopy technique was used to verify the successful incorporation of CTA1 and CTA2 groups into polymer samples. Comparison of the FT-IR spectra of CTA1 and PMMA produced via CTA1-mediated RAFT is presented in **Fig. S8a**, whereas CTA2 and PMMA produce via CTA2-mediated RAFT in **Fig. S8b**. The characteristic peaks of PMMA are observed in both polymer samples, as shown in **Figure 8S**. Hence, the FT-IR characterization of PMMA was included for reference. According to the data reported in refs. [5, 6,7,8], the intense peak at 1723 cm^{-1} in FT-IR spectra of PMMA is assigned to the C=O stretching vibration of the ester group, whereas the two doublet bands occurring at 1143/1190 cm^{-1} and 1240/1267 cm^{-1} correspond to the C-O stretching vibrations of ester groups. The bands located at 1435 and 1480 cm^{-1} are associated with the asymmetric bending vibrations of ($C\text{-}CH_3$) and ($C\text{-}CH_2$) bonds, respectively. The C-C-O stretching vibrations of the methyl carbonyl group are observed at 1267 and 1240 cm^{-1}, whereas the C-O-C vibrations are found at 1190 to 1143 cm^{-1}. The absorption features below 1000 cm^{-1} are due to the C-H rocking modes and C-C skeletal mode[4,5,6,7]. In the higher frequency region of the PMMA spectrum, the intensive C–H symmetric and asymmetric stretching peaks are located between 2800 and 3100 cm^{-1} (2842, 2950 and 2994 cm^{-1}). This region contains the absorption bands assigned to the C–H stretching vibrations of the methyl carboxyl and chain methyl pendant groups, as well as the main chain methylene (CH_2)[4,5,6,7].

In the IR spectrum of CTA1, the most characteristic peak due to the stretching vibrations of the $C \equiv N$ bonds appears at 2243 cm^{-1} (**Fig. S8a**). The bands between 1600-1400 cm^{-1} are mainly assigned to the in-plane ring C=C and C=N stretching vibrations[8]. The C=S and C-S stretching vibration bands are found at 1098 and 833 cm^{-1}, respectively. The

weak peaks occurring above 3010 cm^{-1} are related to the aromatic C–H stretching vibrations while the intense signals below 3010 cm^{-1} are ascribed to the asymmetric and symmetric C-H stretching vibrations of two methyl groups. For polymer sample 4, the existence of the vibrational band of weak intensity at 2245 cm^{-1} was noticed (**Fig. S8a**). This peak is attributed to the C≡N stretching vibrations of the terminal cyano groups of CTA1 units and strongly confirms the presence of CTA1 in the polymer structure. Comparing IR spectra of CTA1 and polymer, we observe the characteristic absorptions originating from both CTA1 and PMMA components in the whole spectral range. In the lower frequency region, many absorption signals typical of CTA1 structure are visible, i.e. the doublet at 1561 and 1583 cm^{-1} or the bands between 1400-1300 cm^{-1} and those below 1000 cm^{-1}. Moreover, a peak at 2918 cm^{-1} is associated with the C–H stretching vibrations of CTA1 units. On the other hand, the peaks at 2956 cm^{-1} and 1706 cm^{-1} correspond to the C-H and C=O stretching vibrations of PMMA units in the synthesized polymer.

For CTA2, the intensive bands in the IR spectrum occurring at 1702 and 1064 $cm^{-1}$are assigned to the stretching vibrations of the C=O and C=S bonds, respectively (**Fig. S8b**)[9,10]. The broadband between 3300-2400 cm^{-1}, originating from the O-H stretching vibrations of hydroxyl groups, is distorted by the strong peaks related to the C–H stretching vibrations (3000-2400 cm^{-1}). An intense peak at 815 cm^{-1} is connected with the stretching vibration of the C-S bonds[8,9]. It can be emphasized that the peak located at 804 cm^{-1}, associated to the stretching vibrations of the C-S groups of CTA2 moieties, confirms that the targeted structure was synthesized successfully.

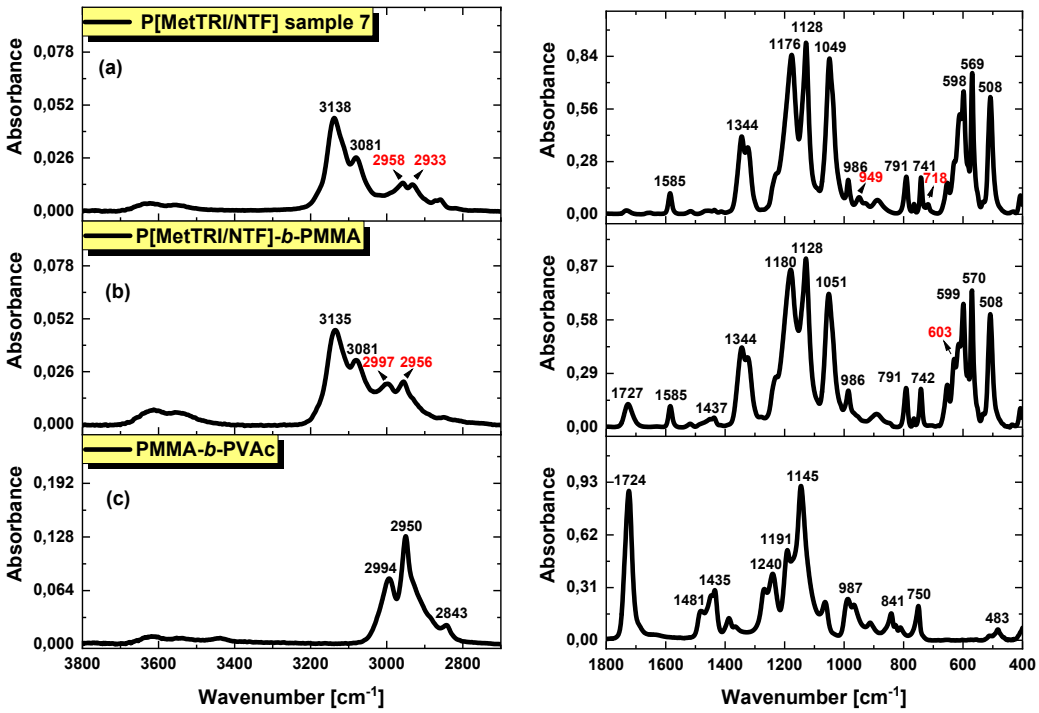

Figure S9. FTIR spectra of (a) P[MetTRI/NTF] sample (b) products of their chain extension *via* MMA polymerization and (c) product of chain extension of PMMA *via* Vac polymerization presented in the spectral range of 3800-400 cm^{-1}.

The presence of the peaks at 949 cm^{-1} and 718 cm^{-1} in the spectrum of P[MetTRI/NTF] (sample 7) indicates that CTA1 units are incorporated into the polymer chains. The signal at 603 cm^{-1} in the spectrum of P[MetTRI/NTF]-*b*-PMMA also origins from the CTA1. The peak observed at 1727 cm^{-1} in the spectrum of P[MetTRI/NTF]-*b*-PMMA sample, corresponding to the C=O stretching vibrations, indicates a successful MMA polymerization process.

The vibrational frequencies observed in the infrared spectrum of the PMMA-b-PVAc sample are very similar to those observed for the PMMA polymer. The most dominant band at 1725 cm^{-1} is due to the C=O stretching vibrations while the two less intense peaks at 1435 and 1387 cm^{-1} are related to the C-H bending vibration of methyl group of PVAc skeleton, respectively. The second most intense band observed at 1145 cm^{-1}, complemented by the peaks at 1191 and 1064 cm^{-1}, are connected with the C-O and C-C stretching vibrations. The most important difference for PMMA and PMMA-b-PVAc polymers appears in the spectral region of ca. 800 cm^{-1}. For PMMA, only one peak occurs at 804 cm^{-1}, while for PMMA-b-PVAc a doublet at 827 and 811 cm^{-1} is present. This is due to the presence of the C-O-C moiety in the backbone of the PMMA-b-PVAc polymer. Moreover, in the case of the PMMA-b-PVAc sample, there is no peaks at 1096 cm^{-1} and 860 cm^{-1} compared to the PMMA polymer.

The molecular structure of the outermost layers of the polymers (sample 13 and 4) was investigated with the use of Time of Flight Secondary Ion Mass Spectroscopy (TOF-SIMS). Through the detection, in the negative mass spectra, of the characteristic for the PMMA molecular species, the presence of PMMA was confirmed for both samples. The intensity of characteristic for PMMA peaks for sample 13 was lower than for 4, which could result from different morphology of the surface of both samples and different charge compensation parameters. Selected characteristics for PMMA peaks were marked on **Fig. S10a** (see ions marked black). In addition, peaks related with substituents characteristic for a given sample are presented in narrowed ranges on **Fig. S10b**(1-3).

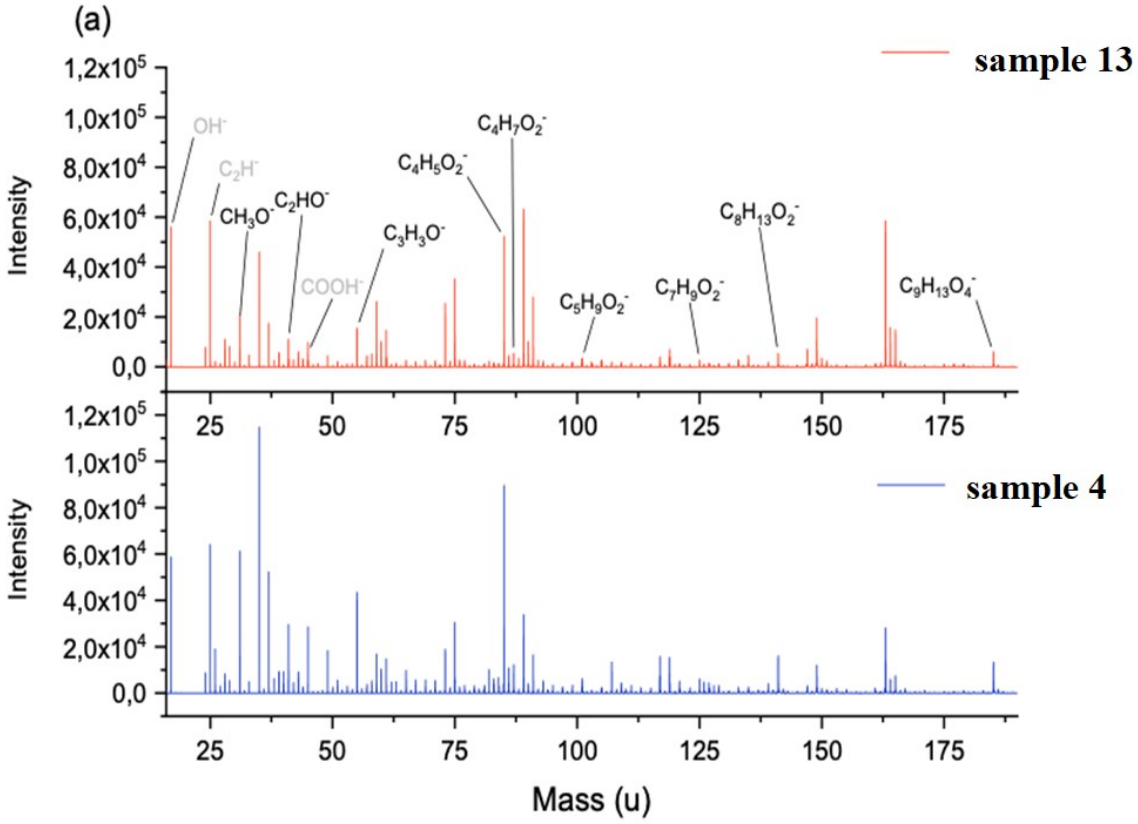

Figure S10a. Negative TOF-SIMS spectra for samples S6 and S13 presented in 16-190 (u) mass range.

$COOH^-$ ion was detected in both samples, and it results from the fragmentation of PMMA compound due to the bismuth ion beam bombardments. Increase of the intensity of this peak (relative intensity ratio when comparing to other PMMA related ions) was not observed for the sample 13. However, analyzing relative intensity ratio of OH- and one of the characteristic signals for PMMA – for example $C_4H_5O_2^-$ an increased intensity of OH- signal is clear.

Presence of sulfur was confirmed for both samples (see **Fig. S10b1**) through the detection of S- ion. The analysis of the nitrogen related ions showed the presence of a small amount of NH^- ions for the sample 13 and lack of it for the 4 (not shown). The CN^- ion was detected for both samples. However, the intensity of this signal for the sample 13 was rather low (see **Fig. S10b2**). Additionally, for the sample 4 CNS^- ion was detected, whereas for the 13 was absent (see **Fig. S10b3**). This would confirm the presence of nitrogen related substitution.

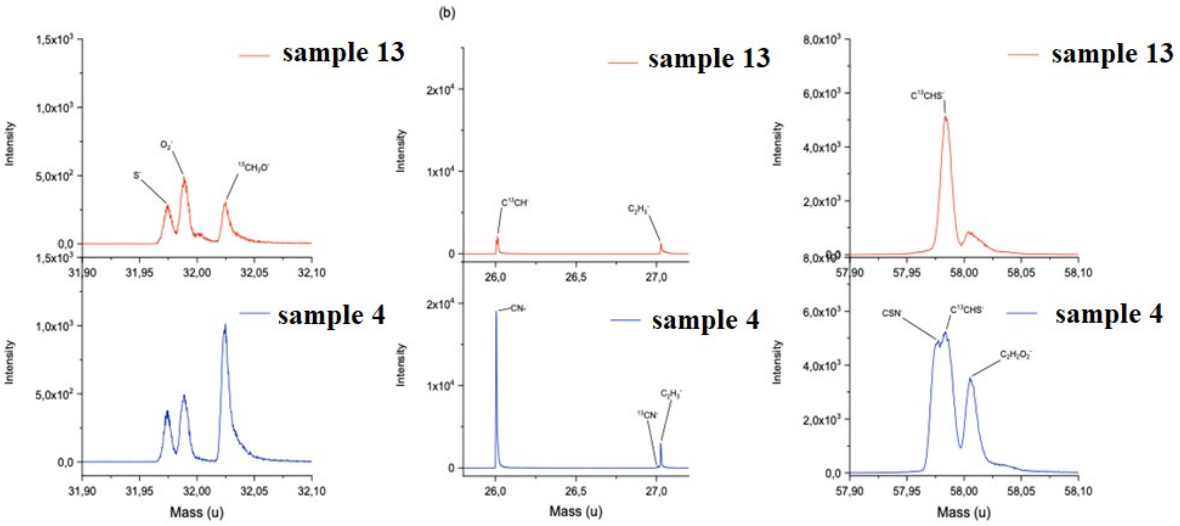

Figure S10b. Negative TOF-SIMS spectra for samples S6 and S13 presented in narrowed mass range: 25.9-27.1 (u), 31.9-32.1 (u), 57.9-58.1 (u).

6. References

[1] W. K. Kipnusu, W. Kossack, C. Iacob, M. Jasiurkowska, J. Rume Sangoro and F. Kremer, *Z. Phys. Chem*., 2012, **226**, 797-805.

[2] https://www.inredox.com/

[3] E. P. Barrett, L. G. Joyn and P. P. Halenda, *J. Am. Chem. Soc.*, 1951, **73**, 373-380.

[4] W. Zhang, J. Yuan, *Macromol. Rapid Commun*., 2016, **37**, 1124-1129

[5] J. Dybal and S. Krimm, *Macromolecules*, 1990, **23**, 1301-1308.

[6] C. P. Ennis and R. I. Kaiser, *Phys. Chem. Chem. Phys.*, 2010, **12**, 14902-14915.

[7] F. Namouchi, H. Smaoui, N. Fourati, C. Zerrouki, H. Guermazi and J. J. Bonnet, *J. Alloys Compd.*, **2009**, 469, 197-202.

[8] P. Tiwari, A. K. Srivastava, B. Q. Khattak, S. Verma, A. Upadhyay, A. K. Sinha, T. Ganguli, G. S. Lodha and S. K. Deb, *Measurement*, 2014, **51**, 1-8.

[9] G. Socrates, *Infrared and Raman Characteristic Group Frequencies: Tables and Charts*, 3rd Edition, John Wiley & Sons Ltd, Chichester, 2001.

[10] P. Maksym, M. Tarnacka, R. Bielas, B. Hachuła, A. Zajac, A. Szpecht, M. Smiglak, K. Kaminski and M. Paluch, *Polymer*, 2020, **192**, 122262.